



MESOPOROUS SILICOALUMINATE MATERIALS (MCM-41, SBA-15 AND MCF) BY ATRANE ROUTE FOR COBALT CATALYST

Received 05 26 2022

Accepted 10 22 2022

Published 10 30 2022

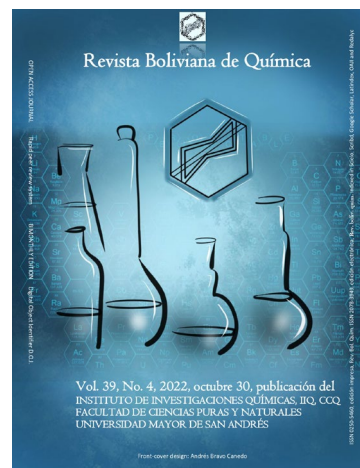
Vol. 39, No.4, pp. 106-125, Sep./Oct.2022

Revista Boliviana de Química

39(4), 106-125, Sep./Oct. 2022

Bolivian Journal of Chemistry

DOI: 10.34098/2078-3949.39.4.2



Full original article

Peer-reviewed

Mauricio Claire Zeballos^{1,2,*}, Fatima L. Pardo Tarifa¹, Luis G. Lopez N.^{1,2}, Saúl Cabrera M.^{1,2†}

- ¹ Laboratorio de Ciencia de Materiales, Instituto de Investigaciones Químicas IIQ, Department of Chemical Sciences, School of Pure and Natural Sciences FCPN, Universidad Mayor de San Andrés UMSA, P.O. Box 303, Calle Andrés Bello s/n-Edificio IIQ, Ciudad Universitaria Cota Cota, Phone +59122795878, La Paz, Bolivia, <http://cienciasquimicas.umsa.bo/>
- ² Instituto del Gas Natural IGN, Universidad Mayor de San Andrés UMSA, P.O. Box 303, Calle Andrés Bello s/n-Edificio IIQ, Ciudad Universitaria Cota Cota, Phone +59122772269, La Paz, Bolivia. sicyt.umsa.bo/unidades/contactoInstituto/103.

Keywords: Mesoporous silicoaluminate, MCM-41, SBA-15, MCF, catalyst support, Cobalt Catalyst

Palabras clave: Silicoaluminatos mesoporosos, MCM-41, SBA-15, MCF, soporte de catalizador, catalizador de cobalto

ABSTRACT

In this work, the synthesis of mesoporous silicoaluminum supports synthesized by the atrane route was performed. The obtained supports presented high homogeneity of the aluminum dispersion, high surface area and narrow pore size distribution. The synthesized mesoporous supports were: MCM-41, SBA-15 and MCF with 10% of Al₂O₃ in the matrix of SiO₂. Twelve percent of cobalt was added to these supports by the incipient wetness impregnation method. These materials were characterized by adsorption of Nitrogen (BET-BJH), Scanning Microscopy Electron (SEM), X-Ray Diffraction (XDR), H₂ Temperature-Programmed Reduction (TPR) and NH₃ Temperature-Programmed Desorption (TPD). According to their structural properties of these catalysts, a promising application in the Fischer-Tropsch syntheses (FTS) is identified.

*Correspondent autor: mauricio.clze@gmail.com



RESUMEN

Materiales silicoaluminatos mesoporosos (MCM-41, SBA-15 y MCF) por ruta atrano para catalizador de cobalto.

Se realizó la síntesis de soportes mesoporosos de silicoaluminato por la ruta del atrano. Los soportes presentaron alta área superficial y alta homogeneidad en la dispersión de aluminio, y estrecha distribución del tamaño de poro. Los soportes mesoporosos sintetizados fueron: MCM-41, SBA-15 y MCF con 10% de Al₂O₃ en la matriz de SiO₂. A estos soportes se les añadió 12% de cobalto por el método de impregnación por humedad incipiente. Estos materiales fueron caracterizados por los métodos de adsorción de Nitrógeno (BET-BJH), Microscopía Electrónica de Barrido (SEM), Difracción de Rayos X (XDR), Reducción a Temperatura Programada de H₂ (TPR) y Desorción a Temperatura Programada de NH₃ (TPD). De acuerdo a sus propiedades estructurales de estos catalizadores, se identifica una aplicación prometedora en las síntesis de Fischer-Tropsch (FTS).

INTRODUCTION

One of the most promising methods for converting coal and natural gas into ultra-clean fuels at an affordable price is the Fischer-Tropsch synthesis (FTS) [1, 2]. For the Fischer-Tropsch synthesis of long-chain paraffins from natural gas, supported cobalt is the chosen catalyst due to its high activity, low water-gas shift activity, and relatively low cost [3, 4]. Alumina, amorphous silica, and titanium oxide are the typical supports for cobalt catalysts in the (FTS) process. However, researchers are currently looking into new catalytic supports, including silicon carbides, carbon nanotubes, and organized silicoaluminate mesoporous supports (MCM-41, SBA-15, and MCM-48 of 1-Dimensional, 2-Dimensional, and 3-Dimensional structures). These novel supports have an advantage over traditional ones due to their large specific surface area for dispersing the active sites and their naturally uniform pore size distribution.

There are several described ordered mesoporous materials in the literature [5]. A 1-Dimensional mesoporous material with an average pore size of 1.5–10 nm is known as MCM-41 (Mobil Composition of Matter, No. 41) [6, 7]. Santa Barbara Amorphous, No. 15 (SBA-15) is a 2-Dimensional mesoporous substance having pores that are typically 2–10 nm in size [8]. Mesoporous MCF (mesoporous cellular foam) is a 3-Dimensional material having pores that range in size from 5 to 50 nm [1]. Aluminum incorporation into a specific mesoporous material has recently been the subject of research [8, 9]. However, few investigations have compared the materials physico-chemical properties when aluminum is added to the mesoporous structure. Aluminum can increase the stability and performance of mesoporous supports for extended periods of time.

In this work, the synthesis of ordered mesoporous silicoaluminate supports like MCM-41, SBA-15 and MCF was developed by the “atrane route” [5,10-11] incorporating 10% w/w of aluminum. Finally, 12% w/w of cobalt was added by the incipient wetness impregnation method. All the materials were characterized by physical and chemical methods and compared to each other. Then, we related the properties, especially the type of acidity (Lewis and Brønsted) and the degree of reducibility.

The aim of this work was to extend the synthesis of mesoporous silica-alumina by the atrane route towards other structures, 1D, 2D and 3D mesostructures. In addition, explore the effect of acidity, pore structure and size of silica-alumina on the final cobalt catalyst.

EXPERIMENTAL

Synthesis of MCM-41 with 10% of structural aluminum

This new method has minor modifications as compared with previously published in S. Cabrera et al. [10]. Initially, the triethanolamine (C₆H₁₅NO₃, TEAH₃) was heated to 140°C, then it was added to a 1M NaOH solution. Then, the mixture was stirred at a constant temperature of 140°C. After, the tetraethyl orthosilicate (Si(OC₂H₅)₄, TEOS) and aluminum isopropoxide (Al(C₃H₆OH)₃, IPA) were added. The mixture was then heated to 140°C maintaining this temperature for 30 minutes. Subsequently, the temperature was lowered to 80°C to add Cetyl trimethylammonium bromide (C₁₉H₄₂BrN, CTAB). After that, the temperature was reduced to 50°C, and water was added and stirred for 2 hours. The mixture was then subjected to a hydrothermal treatment at 100 °C for 24 hours. The molar composition of the reaction mixture was SiO₂: Al₂O₃: TEAH: CTAB: NaOH: H₂O equal to 0.89: 0.054: 3.46: 0.27: 0.23: 82.34.

As a result of the reaction, the solid mixture was then filtered at room temperature, then, the solid was washed with methanol and water, and allowed to dry overnight. A thermal treatment was applied afterwards as follows: The filtered and dried solid was calcined with a ramp of 2°C/min up to 80°C maintaining that temperature for 4 hours. Then, it was heated with the same speed to 120°C for 3 hours. Subsequently, it was heated with the same speed to



220°C for 4 hours. After that, the temperature was raised to 350°C for 4 hours, and then, the temperature was raised to 600°C and kept for 5 hours. The support thus obtained was named as MCM-41Al.

Synthesis of the silatrane-alumatrane complex: precursor of SBA-15 and MCF

Before the synthesis of mesoporous supports SBA-15 and MCF, the atrane complex of silicon and aluminum was prepared [10]. Initially TEAH₃ was heated to 140°C, then, tetraethyl orthosilicate (TEOS) and (IPA) were added. After that, the mixture was heated to 140°C keeping this temperature for 30 minutes.

SBA-15 with 10% of structural aluminum

The method has minor modifications as compared with previously published in Pardo et al. [5]. Initially, 9.38 g of Pluronic triblock copolymer (HO(CH₂CH₂O)₂₀(CH₂CH(CH₃)O)₇₀(CH₂CH₂O)₂₀H) (P-123) and 40 ml of concentrated HCl were dissolved in 270 ml of distilled H₂O. Then, the solution was stirred for 3 hours at room temperature. After that, 0.89 g of Ammonium fluoride (NH₄F) was added. After, the solution was stirred for 30 minutes at room temperature, 5.6 ml of trimethylbenzene (C₆H₃(CH₃)₃) (TMB) was added and stirred for 1 hour at 40°C. Then, silicoalumatrane was added and stirred for 30 minutes at 40°C. Subsequently, it was aged at 100°C for 24 hours without stirring. The molar composition of the reactive mixture was SiO₂: Al₂O₃: TEAH₃: P-123: TMB: NH₄F: HCl: H₂O equal to 0.89: 0.054: 3.43: 0.019: 0.58: 0.11: 5.74: 178.39. After the aging stage, the batch mixture was cooled down to room temperature and washed with distilled water. Then, it was washed with a 50/50 V/V of water and ethanol, and lastly, it was washed only with ethanol. Afterwards, the mixture was filtered, and the remaining solid was dried overnight at 60°C. Finally, the solid product was calcined following the same thermal treatment as described above in the section for the production of MCM-41, with 550°C as the final temperature. The material thus obtained was named as mesoporous support SBA-15Al.

MCF with 10% of structural aluminum

The synthesis method was similar to SBA-15Al with the following modifications: The amount of ammonium fluoride is 2.67g and the amount of (TMB) is 16.8ml. The molar composition of the reagent mixture was: SiO₂: Al₂O₃: TEAH₃: P-123: TMB: NH₄F: HCl: H₂O equal to 0.89: 0.054: 3.44: 0.019: 4.38: 0.87: 5.76: 178.90. The support obtained was named as MCF10Al.

Cobalt impregnation on mesoporous supports

For all the synthesized mesoporous silatrane-alumatrane supports, cobalt was added by the pore volume technique [2, 8]. A nominal weight percentage of 12% of Co was added to the supports from an aqueous solution of cobalt nitrate (1.2 M Approximately). The impregnated supports were dried at 70°C overnight. Then, they were calcined as follow: till 120°C for 4 hours, heated up to 220°C for 4 hours, and finally heated up to 350°C for 6 hours. All the mentioned steps were done at a rate of 2°C/min. The catalysts obtained were named as Co/MCM-41Al, Co/SBA-15Al, and Co/MCF10Al for each of the prepared supports, respectively.

Support and catalyst characterization

The nitrogen adsorption/desorption isotherms were performed at a constant temperature of -196°C in a surface analyzer Autosorb iQ from Quantachrome Instruments. The surface area was obtained by means of the BET (Brunauer-Emmet-Teller) method, and the volume and pore size distribution was obtained by means of the BJH (Barrett-Joyner-Halenda) method. The SEM images were obtained in a Philips XL-30 electron microscope equipment SEM that operates at a voltage of 15 KV with last minute resolution of 1 μm and a magnification range of 200X to 5000X. The X-ray diffraction analysis (XRD) was performed on a Panalytical instrument equipped with a goniometer and a Cu lamp (Kα line, λ=1.5406 Å). The analysis program includes a sweep angle: 10° ≤ 2θ ≤ 90°. The average particle size of Co₃O₄ in calcined samples was calculated using the Scherrer equation from the most intense Co₃O₄ peak at 2θ= 36.9° in the XRD pattern. The obtained Co₃O₄ particle size could be used to calculate the diameter of metallic Co⁰ crystallite after reduction by the following formula [3].

$$d(\text{Co}^0) = 0.75 d(\text{Co}_3\text{O}_4)$$

The analysis of desorption at programmed temperature TPD of ammonia was carried out in a ChemBET TPR/TPD from Quantachrome Instruments. About 0.1g of sample was placed in a U-quartz tube. The sample was



degassed with a Nitrogen flux (N_2 5.0 ultra High Purity) of 70 ml/min at 250°C for about 1 hour. This sample is then activated with a flow of Helium (He 5.0 ultra High Purity) of 70 ml/min with a heating ramp of 10°C/min up to 500°C, and keeping this temperature for 30 minutes. Subsequently, the temperature is lowered to 100 °C and a flow of ammonia (5% V/V of NH_3/He) of 50 ml/min is passed, allowing the ammonia to adsorb in the sample for 1 hour. The ammonia physically adsorbed is then removed for 1 hour at 100°C with the He flux. Finally, the TPD analysis with helium flow of 70 ml/min is performed, increasing the temperature with 10 °C/min up to 800°C and keeping it at this temperature for approximately 60 min. For the TPD analysis of the catalysts, prior analysis, the catalyst was activated with dilute Hydrogen flux (5% V/V H_2/N_2) of 70 ml/min with a temperature ramp of 10 °C/min up to 500 °C and kept at this temperature for 20 min before the analysis.

The TPR programmed temperature reduction analysis was carried out on a ChemBET TPR/TPD equipment from Quantachrome instruments. About 0.1 g of sample was used in a U-quartz tube, the sample is degassed with nitrogen flow (N_2 5.0 ultra High Purity) of 70 ml/min at 250°C for about 1 hour. Afterwards, the temperature was lowered to 20°C and then the TPR analysis of the cobalt catalysts was carried out with diluted hydrogen flow (5% V/V H_2/N_2) of 70 ml/min with a temperature ramp of 10°C/min up to 900°C and kept at this temperature for 20min.

RESULTS AND DISCUSSION

The route of the atranes for different support type MCM-41, SBA-15 and MCF

Nitrogen Physisorption (BET-BJH)

MCM-41 and MCM-41Al

The adsorption/desorption isotherm of MCM-41Al support is shown in figure 1, where the completion of the monolayer is between 0.0 to 0.2 in P/P_0 . Multilayer formation is between the 0.2 to 0.4 fraction. This support is compared with the isotherm of MCM-41 previously reported in literature [5, 12]. The constant curves of the completely filled pores can be observed from 0.4 to 0.95 for MCM-41Al, and from 0.4 to 0.9 for MCM-41. The 0.95 and 0.90 P/P_0 fraction corresponds to the content of interparticle pores. The addition of water promotes the hydrolysis processes that are necessary for the creation of these supports in basic media (Thermodynamically favored) [6, 10]. However, the polymerization decreases when silatrane and alumatrane are used as sources of Si and Al, mainly due to the steric effect of the atrane complexes. Subsequently, the polymerization of Si and Al slows down. Then, due to the loss of ethanol in the silatrane and alumatrane complexes, these final oligomers would be negatively charged. Thus, they would be placed on the surface of the surfactant formed by CTA^+ aggregates that agree with negatively charged oligomers. This would form a micellar surfactant coated with silica and/or alumina [5, 11, 13]. However, in the case of MCM-41Al support, during this process, monomers, dimers, trimers and oligomers might be formed from only aluminum atoms. Because of their negative charge density, they might be added more quickly to the micellar surface of CTA^+ , which would result in the final product having extra-framework regions of aluminum oxides. The addition of aluminum inside and outside the structure could have decompensated the charges during the formation of the final pores. This could be the cause of the variation in the hysteresis of the adsorption/desorption curves in the MCM-41Al support in relation to the MCM-41 support.

The addition of aluminum in the structure of the mesostructured support would involve a decrease in surface area, and an increase in the size of the walls of the structure, as well as a greater distortion in the uniformity of the pore size distribution (See table 1). This may be because of two reasons: The first, to compensate for the surfactant load, the adequate inorganic polyanion would increase as the Al content increases. The second reason may be that as much as the system involves two different elements, there will be a diversity of inorganic polyanions that could contribute to such a load balance.[6]

Hysteresis loops were observed in most isotherms of the mesoporous materials studied in the present study (Figure 1) and (table 1), even though there might not be a clear reason in every case. However, it is generally attributed to a thermodynamics factor and the network effect of the pore system. The thermodynamics factor is related to the metastability of the adsorption and desorption branches. In other words, capillary condensation and evaporation shift towards lower and higher pressures, respectively, relative to the one at which gas and liquid nitrogen (N_2) coexist. For example, for a large pore connected to several other small pores, adsorbates could not desorb at the pressure at which its pore size is. This is because the small connected pores have been filled with the liquid containing the adsorbates. Indeed, the network effect is considered to be the main cause of the hysteresis loops [14].



Another illustration of this may happen in capillary condensation within the so-called "ink-bottle" formed pores, i.e. having an entrance distance across smaller than the estimate of the pore body. Condensation happens continuously in such pores until the pores are totally filled by the condensable vapor at high relative pressures. However, when the relative pressure decreases, the fluid should go out of the pores and thus has to pass through the narrow necks. This happens at a lower relative pressure than what was required for filling the pores, and when the critical relative pressure is come to, the pores empty quickly. Subsequently, a loop in the isotherms shows up [14].

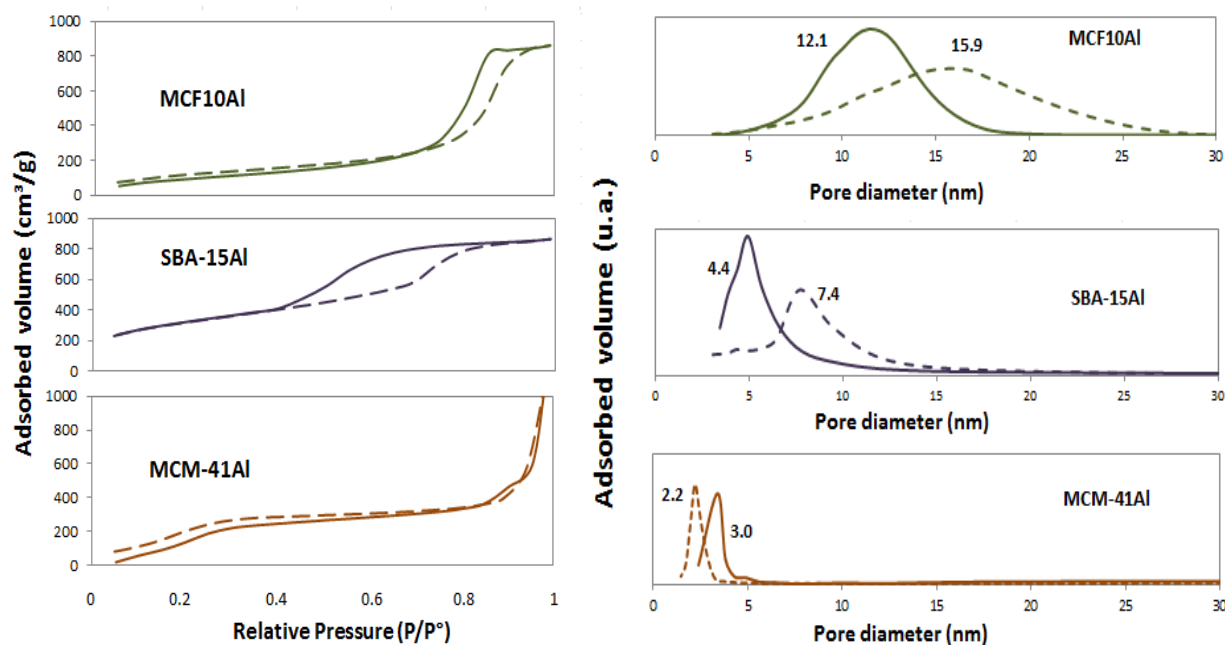


Figure 1. Nitrogen adsorption-desorption isotherms and pore size distribution of mesoporous supports: MCF10Al, SBA-15Al, MCM-41Al.

SBA-15 and SBA-15Al

The adsorption/desorption isotherms of the SBA-15Al support is shown in figure 1. This isotherm is compared with the previously reported SBA-15 support [15-17]. The shape of the isotherms is divided into four parts: The first part of the isotherm of this material is at a relative pressure (P/P_0) between 0 and 0.2, where there is a completion of the monolayer. The second part of the isotherm is at a relative pressure (P/P_0) of 0.2 to 0.4, which is due to the formation of multilayers. The third part of the isotherm is at a relative pressure (P/P_0) between 0.4 and 0.9 for the SBA-15Al support and 0.70 to 0.90 for the SBA-15 support. The type of hysteresis loop that is observed in this material is between types H2 for SBA-15Al and H1 for SBA-15. The deformation of the isotherms of the SBA-15Al support compared to the SBA-15 material might be due to the presence of Aluminum. Finally, the last part of the isotherm, which is at a relative pressure between 0.9 and 1, is similar to the terminations of the H1 and H2 type loops [14]. The deformation of the hysteresis of the support may be due to the existence of tetrahedral aluminum found inside the structure, and octahedral aluminum that would be found outside the structure. [8]. This variation also affects the result of pore volume and surface area distributions.

The micellization of the triblock copolymers (P-123) is driven by the hydrophobic polyethylene oxide (PO) block. The triblock copolymer consists of a core PO block and an ethylene oxide, (EO), block crown. The hydrophilic part, EO, will attract the anionic oligomers of oxohydroxo-Si, thus, forming the condensation of silicon and/or aluminum in the micelles. When TMB is added to the synthesis, it prefers to self-assemble into the hydrophobic core of PO, which causes the micelles to swell [16]. Finally, the addition of the swelling agent (TMB) could affect the equilibrium formation of surfactant micelles and produce disorganized materials. Hence, in an acid medium it is suggested to use silicon and aluminum atrane complexes as metallic precursors [5]. However, as in the case of MCM-41, part of the aluminum might enter the structure and another part of the aluminum may form aluminum oligomers



that would be added more quickly. Therefore, this could occasionally cause variations in the formation of the pores of the SBA-15.

For this same reason, there is also a slight inclination in the hysteresis of nitrogen adsorption and desorption branches (see Fig. 1).

MCF and MCFAl

The adsorption/desorption isotherm of MCF10Al is shown in figure 1. This isotherm is compared to the adsorption/desorption isotherm of MCF support previously reported in literature [1, 5, 18]. The shape of the isotherms is divided into four parts: The first part of the isotherm is at a relative pressure (P/P_0) between 0 and 0.15. The second part of the isotherm is at a relative pressure (P/P_0) of 0.15 to 0.7, which belongs to the formation of multilayers. The third part of the isotherm is at a relative pressure (P/P_0) between 0.7 and 0.94 for the MCF10Al support and 0.7 to 0.98 for the MCF support. The hysteresis loops type is of the H1 type for both supports (See Fig. 2). This isotherm tends slightly to the H3 type for the MCF10Al support, generating a deformation of the isotherm compared to the MCF support isotherm that may be due to the presence of Aluminum. Finally, the last part of the isotherm, which is at a relative pressure (P/P_0) between 0.94 and 1, corresponds to a termination similar to the H1 type loops. As in the SBA-15Al support, the inclination of the hysteresis of the MCF10Al support may be due to the existence of tetrahedral Aluminum that is inside the structure, and to octahedral aluminum that would be found in the extra-framework [8]. This wider variation in nitrogen capillary condensation (hysteresis inclination) implies a greater extension in the pore size distribution, and in turn, this also affects the result of pore volume and surface area distributions [14].

According to these nitrogen adsorption/desorption curves (BET-BJH), the use of atranes as precursors is important. Since they may have controlled hydrolysis and condensation rates, they decrease and resemble hydrolysis rates and condensation of silatrane and alumatrane. This would have favored the introduction of Aluminum in the structure. [6, 10].

The supports SBA-15Al and MCF present two types of porosity, window and cell, that refer to the internal diameter of the pore (cell), and the diameter of entrance to the pore (window), respectively [19]. The SBA-15 support has 2D hexagonal pores [20], and the MCF has 3D spherical pores [1]. Thus, the specific surface area of the MCF10Al support is smaller than the SBA-15Al because it has a larger pore size.

The specific surface area (see table 1) of the supports have the following sequence: MCM-41Al > SBA-15Al > MCF10Al; 1045.1 m²/g; 974.9 m²/g; 408.5 m²/g, respectively. This is similar to the sequence of the supports: MCM-41 > SBA-15 > MCF: 1200 m²/g; 940 m²/g; 860 m²/g. In the same way, the pore size distribution of the supports (see table 1) MCF10Al > SBA-15Al > MCM-41Al are: 12.1 nm; 4.4 nm and 3.0 nm, respectively. This sequence is similar for the series: MCF > SBA -15Al > MCM-41Al, with the average pore size distribution of: 29.3nm; 7.5nm; and 2.6nm.

Table 1. Specific surface area, pore volume, and pore diameter size distribution of MCM-41Al, SBA-15Al, MCF10Al, and MCM-41* [23], SBA-15* [22] and MCF* [21].

Material	BET surface area (m ² /g)	Pore volume (cm ³ /g)	Pore diameter (window) (nm)	Pore diameter (cell) (nm)
MCM-41Al	1045.1	1.29	3.0	3.0
SBA-15Al	974.9	1.34	4.4	7.4
MCF10Al	408.5	1.60	12.1	15.9
MCM-41*	1160	0.9	3.2	-
SBA-15*	980	1.32	9.0	-
MCF*	625	2.40	17.7	35.5

Table 1 shows the BET surface area and BJH pore size distribution data. These materials were also prepared by the route of the atranes. According to this technique, it can be observed that the materials synthesized by the route of the atranes with the addition of 10% aluminum, retain their typical mesostructured morphology. This may be due to



the fact that during the synthesis, the hydrolysis and condensation of Si and Al was controlled, since the deposition rate of these metals on the surfactants was similar [5].

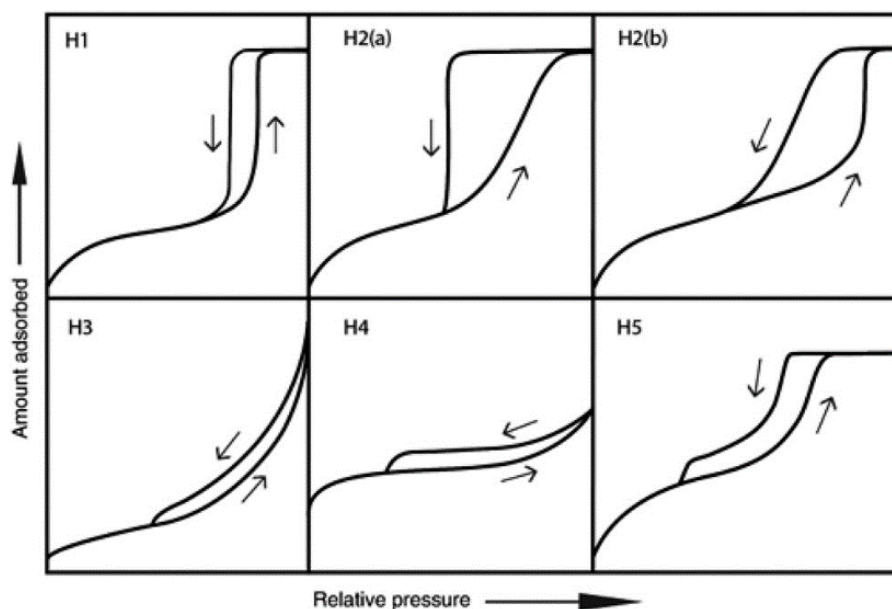


Figure 2. Classification of adsorption-desorption hysteresis loops. Image reproduced by creative commons license [11].

Small Angle X-Ray Diffraction (XRD)

MCM-41 and MCM-41Al

For the MCM-41Al support (see Fig. 3), the characteristic signals can be observed in the 2θ (2 theta) $\approx 2^\circ$ position. This was compared to the data previously reported for the MCM-41 [14, 17]. MCM-41 pattern exhibits the higher signal in 2° (1 0 0). Its secondary signals are in 3.55° (110), 4° (2 0 0) and 5.3° (2 1 0). Analyzing the data, it can be stated that the signals of MCM-41Al has some alteration with respect to the MCM-41 pattern [20] (see Fig. 3). This could be due to the Aluminum load that distorts in some way the defined structure of the pores. For instance, the replacement of silicon by aluminum in the framework favors the formation of tetrahedral aluminum with Al-O(H)-Si bridges, allowing the formation of Brønsted acid sites [9]. For MCM-41Al, secondary signals are also present, although with less intensity.

SBA-15 and SBA-15Al

For the SBA-15Al support (see Fig. 3), the characteristic signal is observed in the 1θ (1theta) $\approx 1^\circ$ position. This support was compared to the data previously reported for the SBA-15 [14, 22]. Its pattern shows the higher signal in 1° (1 0 0), and the secondary signals are in 1.7° (110) and 1.9° (2 0 0). Comparing both supports it is possible to see that the signals of SBA-15Al have some alterations with respect to the SBA-15 pattern. It is possible that the Aluminum load distorts in some way the defined structure of the pores, as explained in the prior part. For SBA-15Al, secondary signals are also observed, although with less intensity.

X-Ray MCF and MCFAl

The MCF pattern, analyzed from literature [14, 18], shows the unique higher signal in $2\theta \approx 0.55^\circ$. On the other hand, for MCF10Al (Se Fig. 3), there is a characteristic signal of the MCF support observed at position 2θ (2 theta) ≈ 0.5 . With this signal, it can be verified that the structure of these supports is in accordance with the results of the nitrogen



adsorption analysis (BET-BJH). However, there is a noticeable distortion between the signals of both supports due to the distortion caused by Al that is produced during the synthesis process.

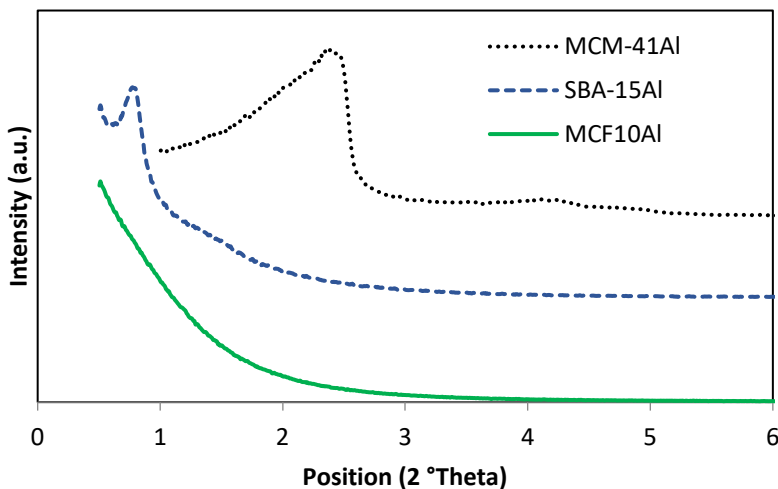


Figure 3. DRX Low angles of MCM-41Al, SBA-15Al and MCF10Al

Temperature Programed Desorption (TPD)

TPD of mesoporous MCM-41Al

The deconvolution of TPD profiles for the mesoporous silicoaluminate MCM-41Al support (see Figure 6.(a)) shows four signals. At low temperature ($\leq 450^\circ\text{C}$) three signals are identified as compared to literature: at 217°C a Lewis weak acidity site which may correspond to the species seen in figure 4 (d); at 285°C , Brønsted weak and medium acidity sites that may correspond to the silanol (Si-O-H) (see figure 4 (b)) with low and medium number of aluminum atoms near to the silicon atom (NNN's); at 365°C a Brønsted strong acidity site, corresponding to Si-O-H, and Si-OH-Al bonds type (see figure 4 (b) (c)) with high number of aluminum atoms near to the silicon atom (NNN's). At high temperature ($\geq 450^\circ\text{C}$) a signal corresponding to Lewis strong acidity site is found at 600°C that might correspond to bonds of aluminum species totally or partially outside of the framework, such as $(\text{AlO})^+$ and $\text{Al}(\text{OH})^{2+}$. Finally, an unidentified signal at 750°C is found.

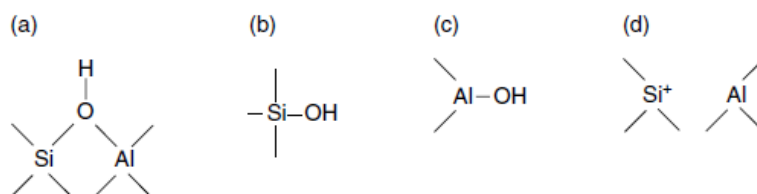


Figure 4. Schematic representation of the different types of hydroxyl groups and acid sites in zeolites. [15]

In aluminosilicate-type zeolites, the 4^+ charge on framework silicon atoms and the 2^- charges on the four coordinating oxygen atoms lead to a neutral tetrahedral framework (SiO_2). If, however, the silicon cation in the framework is substituted by a cation with a 3^+ charge, typically with an aluminum cation, the formal charge on that tetrahedron changes from neutral to 1^- (AlO_4^-). This negative charge is balanced by a metal cation or a hydroxyl proton forming a weak Lewis acid site or a strong Brønsted acid site, respectively. Hydroxyl protons acting as Brønsted acid sites, i.e., as proton donors, are located on oxygen bridges. They connect a tetrahedrally coordinated silicon and aluminum cation on framework positions (Figure 4(a)). These OH^- groups are commonly referred to as structural or bridging OH^- groups (SiOHAl) [23].

The best description of Brønsted acid sites in zeolites is a weakly bound proton of a bridging hydroxyl group between two tetrahedrally coordinated atoms, typically Si and Al. On the other hand, Brønsted acid sites in



amorphous materials are silanol groups involved in a weak interaction with neighboring atoms acting as Lewis acid sites, i.e., as electron pair acceptors, such as Al atoms. [23]

In addition, the impact of the Si–O–T bond angle on the partial charge and the acid strength of the hydroxyl proton has to be considered. In zeolites, the Si–O–T bond angles vary from 137° to 177° for zeolite ZSM-5, from 143° to 180° for mordenite and from 138° to 147° for zeolite Y. Theoretical studies indicate that at a given Si–O–Al bond angle in the local structure of SiOHAl groups, a corresponding partial charge and, therefore, a corresponding acid site with a specific acid strength occurs. [6].

In another theory describing the chemical behavior of aluminosilicate-type zeolites, the aluminum site distribution is considered to be the primary factor affecting the acid strength of SiOHAl groups. The key property is the lower electronegativity of aluminum atoms in comparison with silicon atoms. For example, in FAU-type zeolites, each framework aluminum atom is linked via oxygen bridges with four silicon atoms, which in turn, are connected with nine further T atoms in the next coordination sphere. These nine T atoms in the latter coordination sphere are called next nearest neighbors (NNNs). According to the NNN concept, the acid strength of SiOHAl groups in aluminosilicate-type zeolites depends on the number of framework aluminum atoms on NNN positions. [23] Up till now, the precise chemical nature of Lewis acid sites in zeolites is a subject of research. Lewis acid sites can be attributed to extra-framework aluminum (EFAL) species of octahedral or tetrahedral coordination as well as tri-coordinated aluminum atoms partially dislodged in the framework. Scherzer and co-workers suggested AlO^+ , $\text{Al}(\text{OH})^{2+}$ and $\text{AlO}(\text{OH})$ as EFAL species on extra-framework positions in dealuminated zeolites. Similarly, Kühl *et al.* concluded from X-ray spectrometry that $[\text{AlO}]^+$ units removed from the zeolite framework are transformed into cationic extra-framework species, which act as so-called “true” Lewis acid sites. Framework Lewis acid sites have been suggested to consist of positively charged silicon ions in the neighborhood of tricoordinated aluminum atoms. Elanany *et al.* [24] studied the formation of framework Lewis sites via dehydroxylation routes (a) and (b) in figure 5. Route (b), which contains a defect SiOH group in the vicinity of the bridging OH group, is significantly less endothermic than and, hence, preferred over route (a), which starts with two neighboring bridging OH⁻ groups [6, 23].

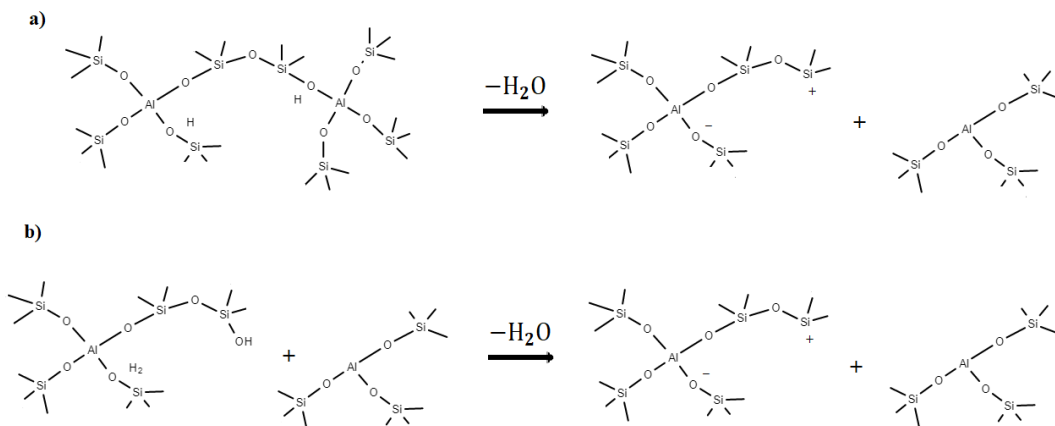


Figure 5. Dehydroxylation mechanisms of zeolites and the formation of Lewis acid sites. Mechanism extracted from 15. Weitkamp *et al.* [15]

TPD of mesoporous SBA-15Al

The deconvolution of TPD profiles for the mesoporous silicoaluminate SBA-15Al support (see figure 6 (b)) shows three signals that were identified by comparison to literature: at 255°C a weak acidity signal, which might correspond to Brønsted and Lewis weak acid sites such as the silanols (Si-O-H) with low number of aluminum atoms near to the silicon atom (NNN's), and the species seen in figure 4(d), respectively. Then, at 425°C a medium acidity signal, which might correspond to a Brønsted and Lewis medium acid site such as the silanols (Si-O-H) with medium number of aluminum atoms near to the silicon atom (NNN's), and alumina species extra-framework such as $\text{AlO}(\text{OH})$, respectively. At 750°C, an unidentified peak that may correspond to a strong acidity site, which might agree with a Brønsted and Lewis weak and strong sites such as: Si-O-H, Si-OH-Al bonds type (see figure 4 (a) (b)) with high number of aluminum atoms near to the silicon atom (NNN's), and species extra-framework such as AlO^+ , $\text{Al}(\text{OH})^{2+}$, respectively. Finally, a no identified signal at 800°C was found.



TPD of mesoporous MCF10Al

The deconvolution of TPD profiles for the mesoporous silicoaluminate MCF10Al support (see figure 6 (c)) shows three signals, that were identified as compared to literature: at 215°C a weak acidity signal, which might correspond to Brønsted and Lewis weak acid sites. These may be silanols (Si-O-H) with low number of aluminum atoms near to the silicon atom (NNN's), and the species seen in figure 4 (d), respectively. At 450°C, a medium acidity signal is observed. This might correspond to Brønsted and Lewis medium acid sites such as the silanols (Si-O-H) with medium number of aluminum atoms near to the silicon atom (NNN's), and alumina species extra framework such as AlO(OH), respectively. At 795°C, an unidentified peak, that might correspond to Brønsted and Lewis strong acid sites such as Si-O-H, Si-OH-Al bonds type (see figure 4 (a) (b)). These have high number of aluminum atoms near to the silicon atom (NNN's). In addition, another peak may correspond to extra framework species such as AlO⁺, and Al(OH)²⁺ respectively. Finally, an unidentified signal at 800°C was found.

According to the Ammonia Programmed Temperature Desorption (TPD) analysis (Figure 6), a high formation of strong acid sites of Brønsted and Lewis can be evidenced. In addition, a lower proportion of strong Lewis and Brønsted acids can be observed.

Table 2 shows the data base of the deconvolution study of the TPD analyzes of the mesoporous supports according to the mesoporous type (MCM-41Al, SBA-15Al and MCF10Al). The silicon/aluminum ratio, remained constant at 7.6. The MCM-41Al support has a higher proportion of weak acids sites than the supports SBA-15Al and MCF10Al according Fig. 6. and table 2. The supports have a higher amount of ammonia adsorbed per gram according to the following order MCF10Al > SBA-15Al > MCM-41Al. In the same way, the dispersion of acid sites per square meter of mesoporous support area ($\mu\text{mol NH}_3/\text{m}^2$) has the following order MCF10Al > SBA-15Al > MCM-41Al. The percentage of accessibility of the acid sites ($(\mu\text{mol NH}_3 \text{ desorbed}/\mu\text{mol of Al in the sample}) \times 100$) has the following sequence from highest to lowest MCF10Al > SBA-15Al > MCM-41Al. This sequence may be due to the species that generate strong, medium and weak Lewis and Brønsted acid sites that are formed in the synthesis process for each one of the supports (seen in this and in the previous section).

Table 2. Adsorption capacity of the mesoporous supports and catalysts

Material	Adsorption of NH ₃ per support mass ($\mu\text{mol/g}$) according to type of acidity			Total adsorption ($\mu\text{mol/g}$)	Dispersion ¹ ($\mu\text{mol NH}_3/\text{m}^2$)	% accessibility to Al ²
	Weak acid	Medium acid	Strong acid			
MCM-41Al	46,1	17,5	66,2	129,8	0,12	6,6
SBA-15Al	9,8	23,6	247,5	280,9	0,29	14,3
MCF10Al	7,2	65,5	252	324,8	0,80	16,6

¹ $\mu\text{mol of NH}_3 \text{ per gram / specific surface area (g/m}^2\text{)}$

²Aluminium in the surface of support / total aluminum

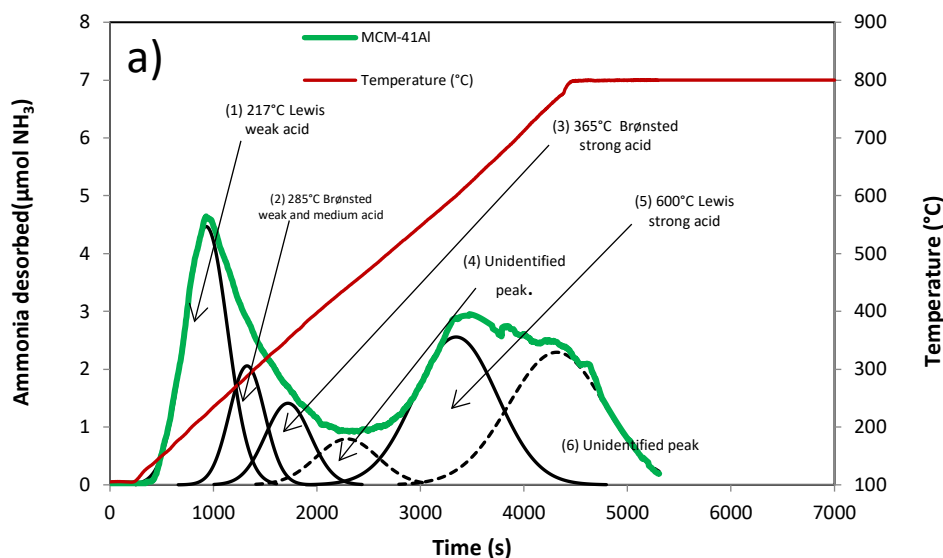


Figure 6. Desorption Temperature-Programmed TPD Profile of support: a) MCM-41Al, b) SBA-15Al and c) MCF10Al

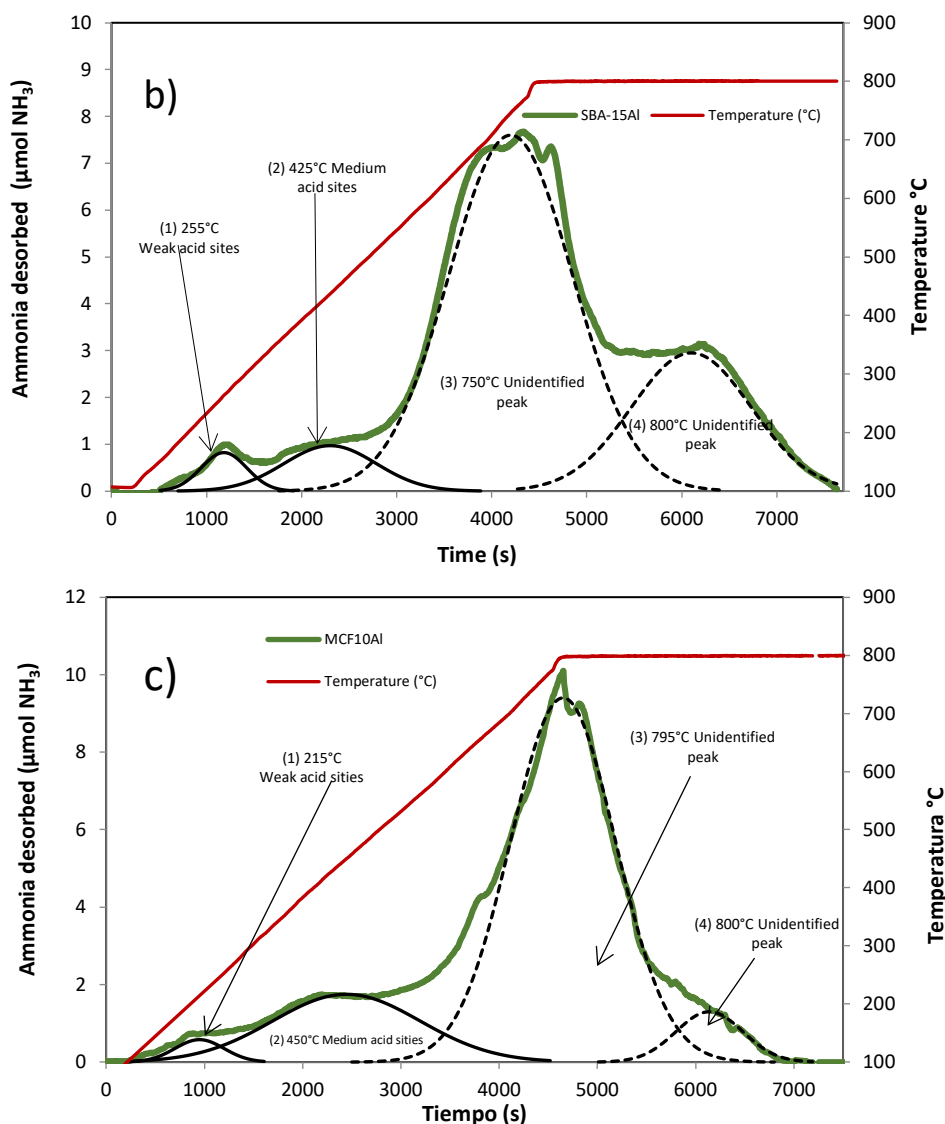


Figure 6 cont. Desorption Temperature-Programmed TPD Profile of support: a) MCM-41Al, b) SBA-15Al and c) MCF10Al

Nitrogen Physisorption (BET-BJH)

MCM-41Al and Co/MCM-41Al

The adsorption/desorption isotherms of the MCM-41Al and Co/MCM-41Al supports are shown in figure 1 and figure 7, where the completion of the monolayer is between 0.0 to 0.2 in P/P_0 . Multilayer formation is between 0.2 to 0.4. The constant curves of the completely filled pores go from 0.4 (for both) to 0.95 and 0.9 for MCM-41Al and Co/MCM-41Al, respectively. And of 0.95 and 0.90 P/P_0 corresponding to the content of interparticle pores. There is a difference in the distribution of pore size and surface area. This may be due to the arrangement of the cobalt particles on the surface of the support particles at the time of the addition of Cobalt and calcining of this material at 350 °C. Another reason may be the pore size and the support-metal interactions. Therefore, this could cause its different surface properties in the material.

SBA-15Al and Co/SBA-15Al

The adsorption/desorption isotherms of the SBA-15Al and Co/SBA-15Al supports are shown in figure 1 and figure 7. The shape of the isotherms is divided into four parts: The first part of the isotherm of these materials is at a relative



pressure (P/P_0) between 0 and 0.2, where there is the completion of the monolayer. The second part of the isotherm is at a relative pressure (P/P_0) of 0.2 to 0.4 for MCM-41Al and 0.2 to 0.55 for Co/MCM-41Al, which is due to the formation of multilayers. The third part of the isotherm is at a relative pressure (P/P_0) between 0.4 and 0.9 for the SBA-15Al support, and 0.55 to 0.92 for the Co/SBA-15Al catalyst. The type of hysteresis loop that is observed in both of the materials is of H2 type. The deformation of the isotherms of the SBA-15Al support compared to the Co/SBA-15Al material might be due to the presence of uniform pore mesostructures.

MCF10Al and Co/MCF10Al

The adsorption/desorption isotherms of MCF10Al support is shown in figure 1 and figure 7. The shape of the isotherms is divided into four parts: The first part of the isotherm is at a relative pressure (P/P_0) between 0 and 0.15. The second part of the isotherm is at a relative pressure (P/P_0) of 0.15 to 0.7 for MCF10Al and 0.15 to 0.6 for Co/MCF10Al, which belongs to the formation of multilayers. The third part of the isotherm is at a relative pressure (P/P_0) between 0.7 and 0.94 for the MCF10Al support, and 0.6 to 0.88 for the Co/MCF10Al catalyst. The hysteresis loop is similar to a H1 type. These isotherms tend slightly to the H3 type, generating a deformation of the isotherm compared to the Co/MCF10Al support isotherm that may be due to the arrangement of cobalt particles.

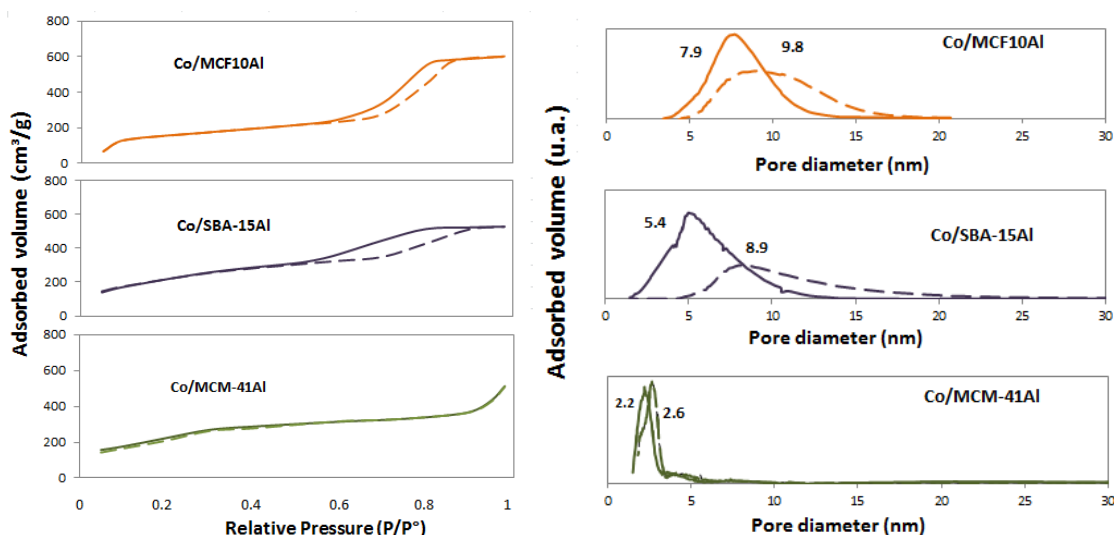


Figure 7. N_2 Adsorption-desorption isotherms and pore size distribution: mesoporous supports with Co

In table 3 and according to figure 7, a summary of the results of the nitrogen desorption analysis of the cobalt catalysts Co/MCM-41Al, Co/SBA-15Al and Co/MCF10Al can be observed, i.e., the surface area, the pore volume, the internal pore size distribution are shown. The average window pore sizes of Co/MCM-41Al, Co/SBA-15Al and Co/MCF10Al are 2.2 nm; 5.4 nm and 7.7 nm respectively. The average internal pore size of Co/MCM-41Al, Co/SBA-15Al and Co/MCF10Al is 2.6 nm; 8.9 nm and 9.8 nm, respectively. The surface area calculated by the BET method, for Co/MCM-41Al, Co/SBA-15Al and Co/MCF10Al is 664.6; 647.5 and 422.1 m^2/g respectively. These surface area results are consistent with the slope in stage 2 of each of the catalyst isotherms. The increase in the specific surface area of the Co/MCF10Al support with respect to MCF10Al might be due to the breakdown of the support structure. And also, this may be due to Cobalt oxide Co_3O_4 nanoparticles on the surface of the support that are not large enough to cover the pores completely, as occurs with Co/MCM-41Al and Co/SBA-15Al. This, increases the surface area of the support with the surface of the Cobalt oxide Co_3O_4 nanoparticles.

Table 3. Surface area, pore volume and pore diameter size distribution of MCM-41, SBA-15Al, MCF10Al, Co/MCM-41Al, Co/SBA-15Al and CoMCF10Al

Material	BET surface area (m^2/g)	Pore volume (cm^3/g)	Pore diameter (window) (nm)	Pore diameter (cell) (nm)
Co/MCM-41Al	664.6	0.69	2.2	2.6
Co/SBA-15Al	646.5	0.99	5.4	8.9
Co/MCF10Al	422.1	0.91	7.7	9.8



X-Ray Diffraction (XRD)

X-Ray Diffraction of cobalt supported catalysts

Figure 8 shows XRD profiles of the cobalt supported catalysts in mesoporous silicoaluminate, which are Co/MCM-41Al, Co/SBA-15Al, Co/MCF10Al. In each of these materials the presence of cobalt oxide Co_3O_4 is observed as the only crystalline phase of cobalt, with signals at angles 2θ (2 theta) of $\approx 31.1^\circ$; 36.9° , 45.0° ; 59.4° and 65.4° (JCPDS: 073-1701). These reflection signals are associated with the planes (2 2 0), (3 1 1), (4 0 0), (5 1 1) and (4 4 0), respectively [2, 5]. These correspond to the cubic system centered on the face of the spinel Co_3O_4 [15, 20]. The Cobalt Co/MCF10Al catalyst has the most intense and sharp cobalt oxide characteristic signals, compared to the Co/SBA-15Al catalyst. In turn, the Co/SBA-15Al catalyst has the cobalt oxide Co_3O_4 characteristic signals more intense and acute than the Co/MCM-41Al catalyst. This could indicate that the catalysts have a crystalline domain size of cobalt particles according to the following sequence from highest to lowest: Co/MCF10Al > Co/SBA-15Al > Co/MCM-41Al. The most intense signal for these materials is at $2\theta \approx 36.9^\circ$. This peak is associated with the plane (3 1 1) [20]. In effect, the crystallite sizes of Co_3O_4 and Co^0 calculated from the Scherrer equation [25, 26] follows the sequence: Co/MCF10Al > Co/SBA-15Al > Co/MCM-41Al (see table 4).

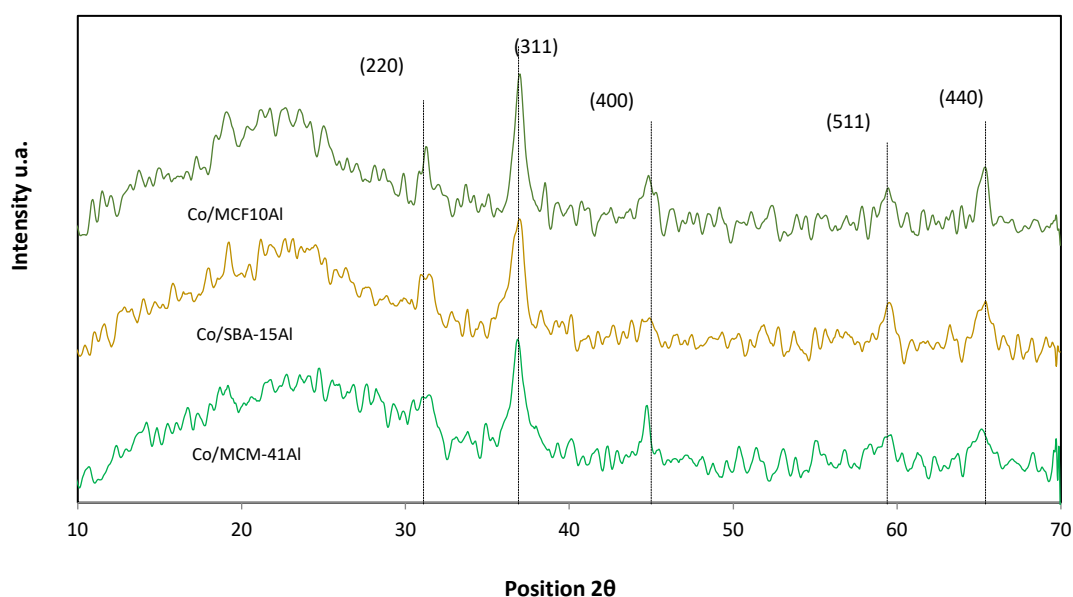


Figure 8. XRD profiles of mesoporous silicoaluminate cobalt catalysts: Co/MCM-41Al, Co/SBA15Al and Co/MCF10Al

In table 4 and according to figure 8, the crystalline microdomain size of the cobalt particles found in the mesoporous silicoaluminate supports is observed. This parameter was calculated with the Scherrer equation [25, 26], which is represented as the diameter of the cobalt crystals in nanometers (nm). This parameter was calculated for the Co/MCM-41Al, Co/SBA-15Al and Co/MCF10Al catalysts. The size of the crystalline microdomain increases when the pore size of the mesoporous supports is larger (see table 4[25]). The crystalline microdomain size distribution has the following sequence: Co/MCF10Al > Co/SBA-15Al > Co/MCM-41Al; 13.3nm > 11.8nm > 10.0nm, respectively. However, the crystal size distribution of Co_3O_4 and Co^0 is larger than the average size of each of the mesostructure types. This may be because the particles of larger metal clusters found on the surface of the support particles produce an increase in the particle size distribution of Co_3O_4 and Co^0 [3].

Table 4. Crystallite size from XRD of Cobalt particles from the Co/MCM-41Al, Co/SBA-15Al and Co/MCF10Al catalysts

Cobalt catalyst	D(Co_3O_4)	D(Co^0) *
Co/MCM-41Al	10.0	7.5
Co/SBA-15Al	11.8	8.9
Co/MCF10Al	13.3	10.0

$$* d(\text{Co}^0) = 0,75d(\text{Co}_3\text{O}_4). [20]$$



Temperature Programmed Reduction (TPR)

Figure 9 shows the Programmed Temperature Reduction signals of the Co/MCM-41Al, Co/SBA-15Al and Co/MCF10Al catalysts. The reduction signals of the three catalysts are divided into two well-marked regions. The first at low temperatures between 280°C and 580°C, and the second is between 610°C and 900°C. The signals at low temperatures represent the reduction reactions from Co_3O_4 to CoO and from CoO to Co^0 . On the other hand, the signals at high temperatures represent the cobalt oxide and minor phases such as silicates and cobalt silicoaluminates that have a strong interaction with the support [1, 2]. The deconvolution at low temperature shows one signal for the reduction from Co_3O_4 to CoO in agreement to the study performed by Claire M. et al. [4], and also, two signals for the reduction from CoO to Co^0 . Cobaltous oxide, CoO, is reduced in two stages: the first reduction is produced on the surface of the cobalt particles, and the second reduction stage is produced on the cobalt that is close to or that has an interaction with the surface of the support [1, 4].

The degree of H_2 consumption in the catalysts in the region of low temperature has the following order: Co/MCF10Al > Co/SBA-15Al > Co/MCM-41Al. The signal for the Co/SBA-15Al is displaced at lower temperatures compared to the other two catalysts. The reduction signal at low temperatures for the Co/MCF10Al catalyst represents the highest H_2 consumption and also, this catalyst has the widest peak at a high temperature. The order of the catalysts for the H_2 consumption in the region at high temperature, from highest to lowest is: Co/MCM-41Al > Co/MCF10Al > Co/SBA-15Al. The reduction signal for Co/SBA-15Al has the lowest intensity. The reduction peak for the Co/MCF10Al has the widest signal at a high temperature compared to the other catalysts.

Regarding the extent of each reduction reaction, the reduction from Co_3O_4 to CoO (temperatures) is similar in the three catalysts as is shown in Table 5. More CoO is reduced to Co^0 in the Co/MCF10Al catalyst compared to Co/SBA-15Al and Co/MCM-41Al catalysts (table 5) specially at low temperature (L) (see Fig. 9). Thus, the reducibility degree decreases in the following order: Co/MCF10Al > Co/SBA-15Al > Co/MCM-41Al. The latter is an important parameter for the application in catalytic reactions such as the Fischer-Tropsch synthesis, i.e., the higher reducibility the higher the activity of the catalyst

Table 5 and figure 9 show the summary of the H_2 consumption data and the deconvolution of the TPR results of the cobalt catalysts Co/MCM-41Al, Co/SBA-15Al and Co/MCF10Al. For the reduction of $\text{Co}_3\text{O}_4 \rightarrow \text{CoO}$, there is no difference of the signal intensity between the three catalysts. For the $\text{CoO} \rightarrow \text{Co}^0$ reduction at low temperatures (L), there is an order of the catalysts for the H_2 consumption as follows: Co/MCF10Al > Co/SBA-15Al > Co/MCM-41Al. For the $\text{CoO} \rightarrow \text{Co}^0$ reduction at high temperatures (H), there is an order of the catalysts for H_2 consumption as follows: Co/MCF10Al > Co/SBA-15Al > Co/MCM-41Al. For the cobalt silicoaluminous zone, the reducibility degree decreases in the following order: Co/MCM-41Al > Co/MCF10Al > Co/SBA-15Al. The cobalt catalyst Co/MCF10Al has the highest degree of reduction with 44.1%, followed by the Co/SBA-15Al catalyst with 39% and the Co/MCM-41Al catalyst that has the lowest reduction percentage of 31%.

The SBA-15 catalyst has larger pore sizes of hexagonal cylindrical shapes, and also a smaller surface area. These pores have a lower proportion of aluminum silicoaluminates than the MCM-41 support. These differences are attributed to the higher surface area and small pore diameter size of the MCM-41, which favors the formation of very small particles that can easily interact with $-\text{OH}$ species present in MCM-41 silica. Cobalt-support interactions in Co/MCF are attributed to the more open network of the silica support which favors the diffusion of Co ions during impregnation and calcination stage. Thereafter, these cobalt ions might reach the window pores in the cell spheres where the probability of interaction with the silanol groups is higher due to the small window pore sizes.

Co/MCM-41Al and Co/SBA-15Al catalysts showed different degrees of reduction. One explanation might be the pore diameter of the silica support. It was reported that smaller pore diameters in mesoporous silica likely form and stabilize smaller cobalt oxide particles with higher dispersion. Nevertheless, the pore diameter of the silica support material is not the only possible explanation for diverse reduction properties [2, 3]. Some authors tried to explain the difference between MCM-41Al and SBA-15Al and found that the pore surface consists of regularly arranged isolated surface SiOH groups [8, 9]. These OH species, in parallel direction to the cylindrical pore axis, are absent in MCM-41. On the contrary, the inner surface of SBA-15 contains isolated and interacting SiOH groups able to form hydrogen bonds with other OH groups as well as geminal $\text{Si}(\text{OH})_2$ groups with all of them pointing in all directions of space. Pore models have shown that the inner surface of SBA-15 is substantially "rougher" than the pore surface of MCM-41 [27]. Therefore, it is reasonable to think that due to the rougher inner surface of the SBA-15 support, the interactions of cobalt particles with silica surface sites in the Co/SBA-15 catalyst are weaker and, as a result, less cobalt-silicate is formed.

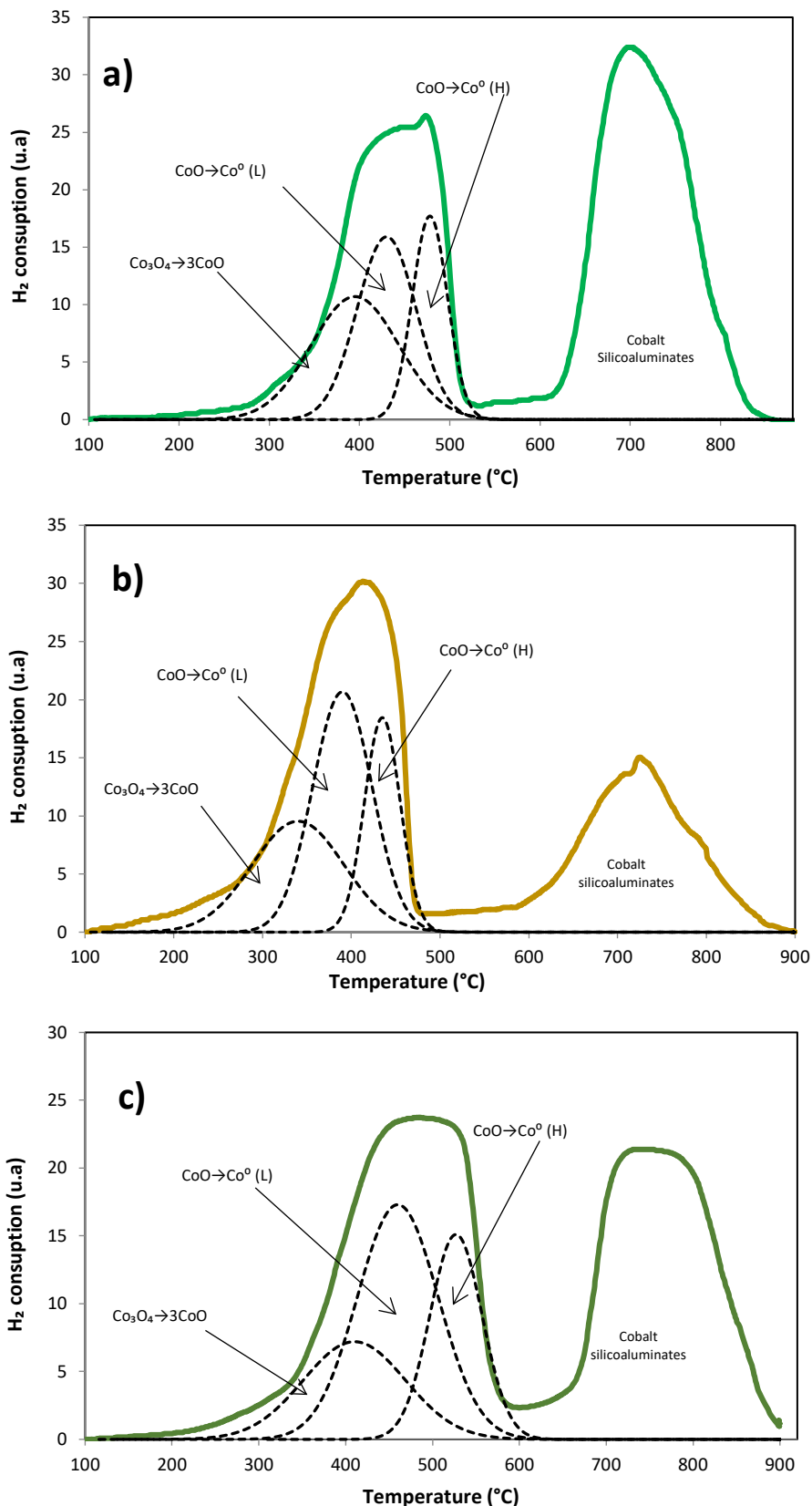


Figure 9. Temperature- Programmed Reduction (TPR) Profile for reduction of catalysts: a) Co/MCM-41Al, b) Co/SBA-15Al y c) Co/MCF10Al



Consequently, the Degree of Reduction (%Reducibility degree) is higher for Co/SBA-15Al than for the MCM-41Al support. It is interesting to note that the degree of reduction is also high for Co/MCF10Al even though it has a high cobalt-silicate formation. The explanation given to this fact is the pore structure and size of the silica. It was reported that water produced during the reduction process (TPD) oxidizes the Co^0 . This effect is more pronounced in catalysts with small and long pores due to water accumulation inside the pores. However, this is not the case for the Co/MCF10Al which has large 3D spherical pores. Moreover, the produced water is easier to diffuse through this network and possibly, there might be less Co^0 oxidation, which can increase the degree of reduction. [11]

Table 5. Hydrogen consumption of cobalt catalysts: Co/MCM-41, Co/SBA-15Al y Co/MCF10Al (based on Co^0)

Material	Consumption of H_2 per catalyst mass ($\mu\text{mol H}_2/\text{g}$) depending on the type of reaction			Silicoaluminates of Co	% Reducibility degree
	$\text{Co}_2\text{O}_3 \rightarrow \text{CoO}$	$\text{CoO} \rightarrow \text{Co}^0(\text{L})$	$\text{CoO} \rightarrow \text{Co}^0(\text{H})$		
Co/MCM-41Al	0,75	0,70	0,60	2,69	31,5
Co/SBA-15Al	0,79	1,13	0,62	1,34	39,0
Co/MCF10Al	0,71	1,38	0,77	2,09	44,1

Cluster accumulation on the catalyst surface and by pore size

Cobalt clusters are accommodated in two different ways on mesostructured or amorphous materials by the method of incipient Wetness[8]. There is a deposition of cobalt clusters on the surface of the support particles, and another fraction is deposited according to the pore size. There are also small clusters that can be deposited indoors inside the pore interstices. So, according to the diffractograms, and using the Scherrer equation, it can be seen that the average size of the cobalt particles is somewhat larger than the diameter of the pores. Ordering the catalysts as a function of their particle size distribution from highest to lowest we have: Co/MCF10Al > Co/SBA-15Al > Co/MCM-41Al

Cobalt-support TPR interaction

The support-metal interactions mainly depend on the size of the pores, the type of pore, the angle of the porous cavity, the type of surface acidity.

Temperature Desorption Programmed (TPD)

TPD of Co/MCM-41Al catalyst

The TPD profiles for the mesoporous silicoaluminate Co/MCM-41Al catalyst (see figure 10 (a)) are similar to the profile of the MCM-41Al support (see figure 6 (a)). At low temperature ($\leq 450^\circ\text{C}$) three signals were identified as compared to literature: at 217°C a signal for Lewis weak acidity sites, at 285°C a signal for Brønsted weak and medium acidity sites, at 365°C a signal for Brønsted strong acidity sites. At high temperature ($\geq 450^\circ\text{C}$) a signal corresponding to Lewis strong acidity sites was found at 600°C , and an unidentified signal at 750°C was found. The latter signal is notably increased by the presence of Cobalt (Co/MCM-41Al catalyst), which might be attributable to Lewis strong acidity of Co^0 [21]. Also, when cobalt is added to MCM-41Al, the total amount of acid sites is increased by three fold as is shown in Table 4. In addition, the dispersion of acid sites is increased by approximately six times when cobalt is added

According to the TPD of the MCM-41Al support (see figure 6 a), this material has a majority fraction of weak Brønsted acid sites and Lewis weak and medium acid sites. This would favor a lower metal-support interactions. Because of this, it would be expected to have a reduced metallic cobalt fraction at a lower temperature, which is true and is shown in Figure 10. However, there are also particles or clusters that were deposited in internal pores cavities and/or had a strong interaction with strong acids. This may be verified by the second band of reduction present at temperatures greater than 600°C . These signals may be due to cobalt silicoaluminates formed by these strong interactions.

TPD of Co/SBA-15Al catalyst

The TPD profiles for the mesoporous silicoaluminate Co/MCM-41Al catalyst (see figure 10 (a)) are similar to the profile of the MCM-41Al support (see figure 6 (a)). At low temperature ($\leq 450^\circ\text{C}$) three signals were identified as



compared to literature: at 217 °C a signal for Lewis weak acidity sites, at 285 °C a signal for Brønsted weak and medium acidity sites, at 365°C a signal for Brønsted strong acidity sites. At high temperature ($\geq 450^\circ\text{C}$) a signal corresponding to Lewis strong acidity sites was found at 600°C, and an unidentified signal at 750C was found. The latter signal is notably increased by the presence of Cobalt (Co/MCM-41Al catalyst), which might be attributable to Lewis strong acidity of Co^0 [21]. Also, when cobalt is added to MCM-41Al, the total amount of acid sites is increased by three fold as is shown in Table 4. In addition, the dispersion of acid sites is increased by approximately six times when cobalt is added.

Unlike MCM-41Al, this support has a higher proportion of acidic sites on the surface, with similar pore size, but with a larger size. This acidity causes greater metal-support interactions. For this reason, the reduction in TPR is shifted to the right, requiring a higher temperature for its reduction. However, it has a greater degree of reducibility. The reason may be that at larger pore sizes, the metal particles are larger and easier to reduce.

TPD of Co/MCF10Al catalyst

The TPD profiles for the mesoporous silicoaluminate Co/MCF10Al catalyst (see figure 10 (c)) shows similar profile to the one of the MCF10Al support (see figure 6 (c)). Three signals are identified as compared to literature: at 215°C a peak for weak acidity sites, at 450°C a peak for medium acidity sites, at 795°C an unidentified peak that it may be of strong acidity sites, and an unidentified signal at 800°C was found. The latter signal is notably increased by the presence of Cobalt (Co/MCFAl catalyst), which might be attributable to Lewis strong acidity of Co^0 . Also, when cobalt is added to MCF, the total amount of acid sites is increased by 63% as is shown in Table 6.

Co/MCF10Al catalyst as in the case of Co/SBA-15Al catalyst, has a large number of strong acids, which increases the metal-support interactions. However, according to the average size of Co particles, Co/MCF10Al has the largest average pore size distribution among the two previous supports. What makes it possible is that despite having a strong support-metal interactions, its cobalt particles are larger, and mostly reducible at a lower temperature and with a greater degree of reducibility.

Table 6 shows the data base of the deconvolution study of the TPD analyzes of the catalysts according to the type of mesoporous (Co/MCM-41Al, Co/SBA-15Al and Co/MCF10Al). The catalysts have a higher amount of ammonia adsorbed per gram according to the following order Co/MCF10Al > Co/MCM-41Al > Co/SBA-15Al. The contribution of acidity due to the presence of cobalt (Co^0) active sites has the following order: Co/MCM-41Al > Co/MCF10Al > Co/SBA-15Al. Similarly, the dispersion of acid sites per square meter of catalyst area ($\mu\text{mol NH}_3/\text{m}^2$) has the following order: Co/MCF10Al > Co/MCM-41Al > Co/SBA-15Al.

Table 6. Adsorption capacity of the mesoporous supports and catalysts

Material	Total adsorption ($\mu\text{mol/g}$)	Dispersion ¹ ($\mu\text{mol NH}_3/\text{m}^2$)	Metal adsorption ³ ($\mu\text{mol/g}$)
Co/MCM-41Al	448,4	0,67	318,5
Co/SBA-15Al	362,3	0,56	81,4
Co/MCF10Al	530,3	1,26	205,5

¹ $\mu\text{mol of NH}_3$ per gram/ specific surface area (g/m^2)

² $\mu\text{mol of metal acidity sites per gram of catalyst}$

For the series of mesoporous type materials supports (MCM-41Al, SBA-15Al, and MCF10Al) and Catalysts (Co/MCM-41, Co/SBA-15, and Co/MCF), the results of nitrogen physisorption show high specific surface area, and a narrow pore size distribution in the order of the mesopores. According to these results, these materials could be suitable as support for Fisher Tropsch catalysts, and catalytic cracking among others. The variation of surface area and pore size distribution in these series depends on the amount of Aluminum inserted in the matrix and the route of synthesis for each one. In the XRD diffractograms of the cobalt catalysts in these series, it is observed that the Cobalt particles were inserted homogeneously in the supports, since there is a single phase of cobalt in the surface of the matrix which is the double oxide of cobalt (Co_3O_4). This property is good for catalysis because the reduction of this cobalt phase is expected at low temperatures. The mesoporous supports and catalysts synthesized by the atrane route show different weak, medium and strong acid species of Lewis and Brønsted. This depends on the amount of Aluminum added, the pore size and the structure being of 1-Dimension, 2-Dimension and/or of 3-Dimension.

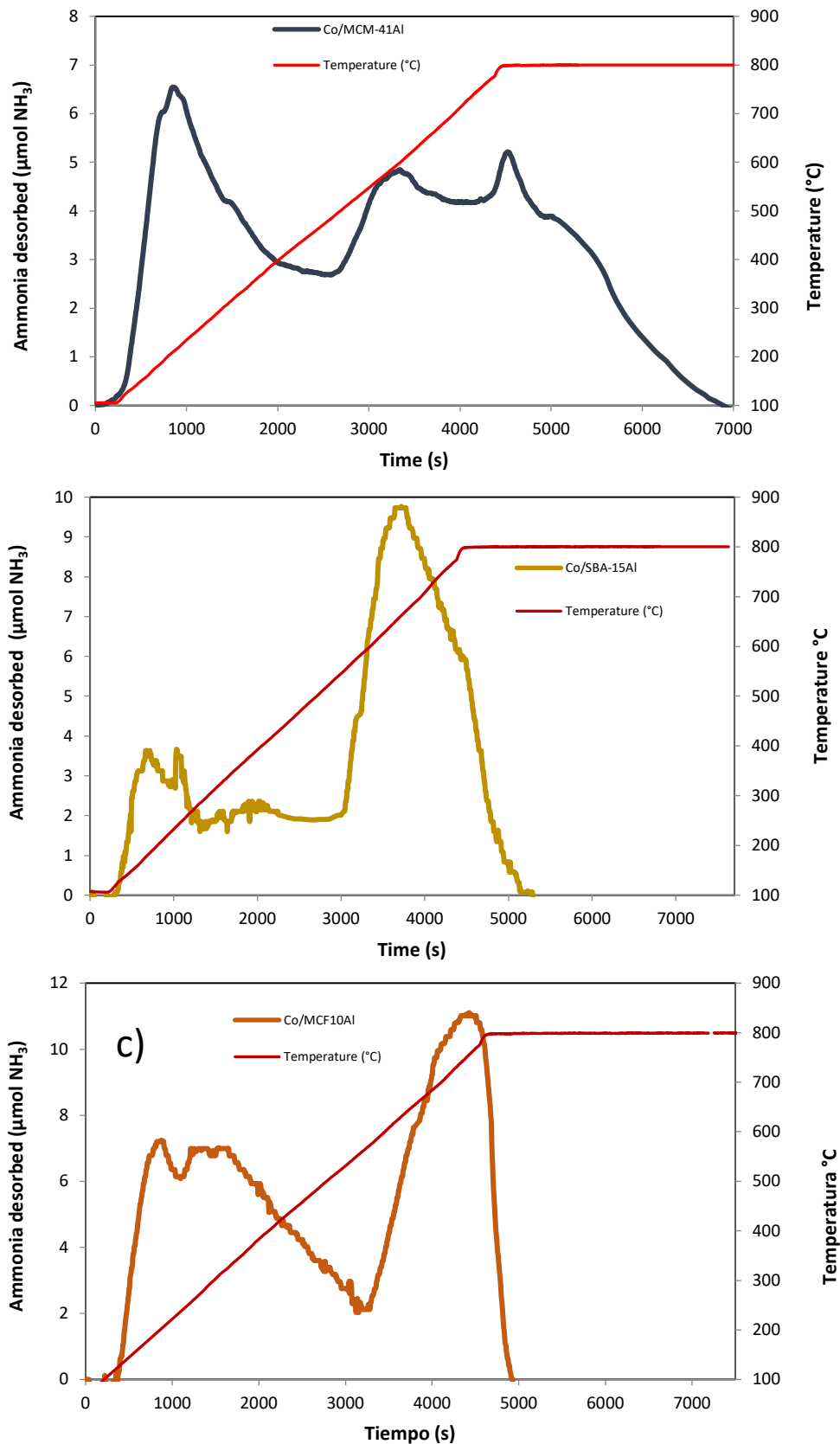


Figure 2. Desorption Temperature-Programmed TPD Profile of catalysts: a) Co/MCM-41Al, b) Co/SBA-15Al and c) Co/MCF10Al



The addition of cobalt to these matrices results in an increase of the acidity of the strong, medium and weak acids of Lewis, which varies according to the type of mesostructure. These Lewis acids are due to the presence of Co^0 that could be related to the catalytic performance of the cobalt active sites. The Co/MCF10Al catalyst has a greater degree of relative reducibility. The total amount of reduction depends on the type of support and the amount of aluminum inserted in the matrix. This property is important for Fischer-Tropsch Synthesis.

CONCLUSION

The new mesoporous silicoaluminate supports synthesized by the atrane route, type MCM-41Al, SBA-15Al and MCF10Al, with high specific surface area and with a narrow pore size distribution in the order of the mesopores were obtained. In the same way, mesoporous supports were obtained with the variation of the amount of aluminum, with similar characteristics.

Cobalt catalysts were obtained, by the incipient wet impregnation method, on the mesoporous supports of silicoaluminates. According to their physical and superficial properties, analyzed by the X-ray diffraction analysis (XRD), a single phase of cobalt oxide (Co_3O_4) was identified. Moreover, the crystalline microdomain size of the cobalt catalysts was calculated by the Scherrer equation to be in a range between 7,5 and 10nm. The TPR programmed temperature reduction analysis of hydrogen was also carried out, where for the series of catalysts by mesoporous type, the Co/MCF10Al catalyst obtained the highest degree of reducibility reaching up to 44.1%. In the case of the MCF catalyst series, with aluminum variation, the Co/MCF10Al catalyst obtained the highest degree of reducibility reaching up to 44.1%. These characteristics are optimal for the Fischer-Tropsch catalytic reactions.

By means of the TPD technique, the total acidity of the mesoporous supports was measured. It was also measured the type and quantity of each of the acids present in the mesoporous supports, the dispersion of the acid sites and the accessibility to these. In addition, the TPD analysis of the cobalt catalysts was performed, where an increase in the weak, medium and strong Lewis acids sites was found. The Lewis acid sites of metallic cobalt might be related to the Fischer-Tropsch catalytic activity. The understanding of this type of correlation as well as its control through the synthesis method is of vital importance to obtain new catalysts with better performance.

ACKNOWLEDGEMENTS

The authors are grateful for financial support from SIDA (Swedish government) in the research project "Energy and Hydrocarbons for Sustainable Development" and for financial support from IDH (Bolivian government) in the project "New catalysts for cracking that favor the production of diesel oil in Bolivia".

REFERENCES

1. Wei, L., Zhao, Y., Zhang, Y., Liu, C., Hong, J., Xiong, H., Li, J. **2016**, Fischer-Tropsch synthesis over a 3D foamed MCF silica support: Toward a more open porous network of cobalt catalysts, *Journal of Catalysis* **340**, 205–218. DOI: <https://doi.org/10.1016/j.jcat.2016.04.019>
2. González, O., Pérez, H., Navarro, P., Almeida, L.C., Pacheco, J.G., Montes, M. **2009**, Use of different mesostructured materials based on silica as cobalt supports for the Fischer-Tropsch synthesis, *Catalysis Today*, **148**(1-2), 140–147. DOI: <https://doi.org/10.1016/j.cattod.2009.03.030>
3. Liu, Y., Hanaoka, T., Miyazawa, T., Murata, K., Okabe, K., Sakanishi, K. **2009**, Fischer-Tropsch synthesis in slurry-phase reactors over Mn- and Zr-modified Co/SiO₂ catalysts, *Fuel Processing Technology*, **90**(7-8), 901–908. DOI: <https://doi.org/10.1016/j.fuproc.2009.04.004>
4. Claire, M. **2017**, Obtención de silicoaluminatos mesoporosos por la ruta de los atranos evaluando sus propiedades acido/base y redox para identificar su potencial aplicación como matrices en procesos catalíticos, (MSc tesis), Universidad Mayor de San Andrés (UMSA), La Paz, Bolivia, retrieved from <https://repositorio.umsa.bo/handle/123456789/17880>
5. Pardo-Tarifa, F., Montes, V., Claire, M., Cabrera, S., Kusar, H., Marinas, A., Boutonnet, M. **2017**, Silica with 3D Mesocellular Pore Structure Used as Support for Cobalt Fischer-Tropsch Catalyst, *Synthesis and Catalysis: Open Access*, **2**(3), 11. DOI: 10.4172/2574-0431.100017
6. Cabrera, S., El Haskouri, Guillem, C., Latorre, J., Beltrán-Porter, A., Beltrán-Porter, D., Dolores-Marcos, M., Amorós, P. **2000**, Generalised syntheses of ordered mesoporous oxides: the atrane route, *Solid State Sciences*, **2**, 405–420. DOI: [https://doi.org/10.1016/S1293-2558\(00\)00152-7](https://doi.org/10.1016/S1293-2558(00)00152-7)
7. Chen, C-Y., Li, H-X., Davis, M.E. **1993**, Studies on mesoporous materials: I. Synthesis and characterization of MCM-41, *Microporous Materials*, **2**, 17-26. DOI: 10.1016/0927-6513(93)80058-3
8. Li, Y., Zhang, W., Zhang, L., Yang, Q., Wei, Z., Feng, Z., Li, C. **2004**, Direct Synthesis of Al-SBA-15 Mesoporous Materials via Hydrolysis-Controlled Approach, *J. Phys. Chem. B.*, **108**(28), 9739-9744. DOI: <https://doi.org/10.1021/jp049824j>
9. Kosslick, H., Lischke, G., Parlitz, B., Storek, W., Fricke, R. **1999**, Acidity and active sites of Al-MCM-41, *Applied Catalysis A: General*, **184**(1), 49-60. DOI: [https://doi.org/10.1016/S0926-860X\(99\)00078-2](https://doi.org/10.1016/S0926-860X(99)00078-2)
10. Cabrera, S. **1999**, Química en medios organizados para la obtención de nuevas alúminas, aluminosilicatos y ALPO's mesoporosos con tamaño de poro modulable, (PhD tesis), Universitat de València, Valencia, España, retrieved from <https://dialnet.unirioja.es/servlet/tesis?codigo=225426>



11. Pardo-Tarifa, F. **2017**, Cobalt catalyst supports for Fischer-Tropsch synthesis, (PhD thesis), KTH Royal Institute of Technology, Stockholm, Sweden, retrieved from <http://www.diva-portal.org/smash/get/diva2:1146405/FULLTEXT02.pdf>
12. Miricioiu MG, Jacob C, Nechifor G and Niculescu, V-C. **2019**, High Selective Mixed Membranes Based on Mesoporous MCM-41 and MCM-41-NH₂ Particles in a Polysulfone Matrix, *Front. Chem.*, *7*, 332. DOI: 10.3389/fchem.2019.00332
13. Ortiz de Zárate, D., Fernandez, L., Beltrán, A., Guillem, C., Latorre, J., Beltrán, D., Amorós, P. **2008**, Expanding the atrane route: Generalized surfactant-free synthesis of mesoporous nanoparticulated xerogels, *Solid State Sci.*, *10*(5), 587-601. DOI: <https://doi.org/10.1016/j.solidstatesciences.2007.10.014>
14. Zhao, D., Wan, Y., Zhou, W. Ordered Mesoporous Materials, Wiley-VCH Verlag GmbH & Co. KGaA, **2013**, Singapore, pp. 138-144. DOI: 10.1002/9783527647866
15. Santos, G.A., Santos, C.M.B., da Silva, S.W., Urquieta-González, E.A., Confessori Sartoratto, P.P. **2012**, Sol-gel synthesis of silica-cobalt composites by employing Co₃O₄ colloidal dispersions, *Colloids and Surfaces A: Physicochem. Eng. Aspects*, *395*, 217– 224. DOI: <https://doi.org/10.1016/j.colsurfa.2011.12.033>
16. Cao, L., Kruk, M. **2010**, Synthesis of large-pore SBA-15 silica from tetramethyl orthosilicate using triisopropylbenzene as micelle expander, *Colloids and Surfaces A: Physicochemical and Engineering Aspects*, *357*(1–3), 91-96. DOI: <https://doi.org/10.1016/j.colsurfa.2009.09.019>
17. Shen, Z., Cai, N., Sue, Y., Yu, B., Wang, J., Song, H., Deng, H., Yu, F. **2020**, Porous SBA-15/cellulose membrane with prolonged antimicrobial drug release characteristics for potential wound dressing application, *Cellulose*, *27*, 2737-2756. DOI: <https://doi.org/10.1007/s10570-020-02967-4>
18. Held, A., Kowalska-Kuś, J., Nowińska, K., Góra-Marek, G. **2018**, MCF Material as an Attractive Support for Vanadium Oxide Applied as a Catalyst for Propene Epoxidation with N₂O, *Catal Lett*, *148*, 2058–2068. DOI: <https://doi.org/10.1007/s10562-018-2420-6>
19. Schmidt-Winkel, P., Lukens, W.W., Yang, P., Margolese, D.I., Lettow, J.S., Ying, J.Y., Stucky, G.D. **2000**, Microemulsion Templating of Siliceous Mesostructured Cellular Foams with Well-Defined Ultralarge Mesopores, *Chem. Mater.*, *12*(3), 686-696. DOI: <https://doi.org/10.1021/cm991097v>
20. Martínez, A., Lopez, C. **2006**, Fischer-Tropsch catalysts based on cobalt supported on ordered mesoporous silicas, *Revista Mexicana de Ingeniería Química*, *5*(3), 167-177. <https://www.redalyc.org/articulo.oa?id=62050301>
21. Schmidt-Winkel, P., Lukens, W., Zhao, D., Yang, P., Chmelka, B.F., Stucky, G.D. **1999**, Mesocellular Siliceous Foams with Uniformly Sized Cells and Windows. *J. Am. Chem. Soc.*, *121*(1), 254-255. DOI:10.1021/JA983218I
22. Tahira, Y., Müller, K. **2016**, Structural characterization of octadecyl modified MCM-41 silica by NMR and FTIR. *J Porous Mater.*, *23*, 339–348. DOI: 10.1007/s10934-015-0086-7
23. Weitkamp, J., Hunger, M. **2007**, Chapter 22 - Acid and base catalysis on zeolites, *Studies in Surface Science and Catalysis*, Institute of Chemical Technology, University of Stuttgart, Stuttgart, Germany., *168*, 787-835, DOI: [https://doi.org/10.1016/S0167-2991\(07\)80810-X](https://doi.org/10.1016/S0167-2991(07)80810-X)
24. Elanany, M., Koyama, M., Kubo, M., Broclawik, E., Miyamoto, A. **2004**, Periodic density functional investigation of Lewis acid sites in zeolites: relative strength order as revealed from NH₃ adsorption, *Applied Surface Science*, *246*, 96–101. DOI:10.1016/j.apsusc.2004.10.052
25. Song, D., Li, J. **2006**, Effect of catalyst pore size on the catalytic performance of silica supported cobalt Fischer-Tropsch catalysts, *Journal of Molecular Catalysis A: Chemical*, *247*(1-2), 206–212. DOI: <https://doi.org/10.1016/j.molcata.2005.11.021>
26. Wattanathana, W., Nootsuwan, N., Veranitisagul, C., Koonsaeng, N., Laosiripojana, N., Laobuthee, A. **2015**, Simple cerium-triethanolamine complex: Synthesis, characterization, thermal decomposition and its application to prepare ceria support for platinum catalysts used in methane steam reforming, *Journal of Molecular Structure*, *1089*, 9–15. DOI: doi.org/10.1016/j.molstruc.2015.02.010
27. Vansant, EF., Van Der Voort, P., Vrancken, K.C. **1995**, The surface chemistry of silica, *Stud. Surf. Sci. Catal.*, *93*, 59-77. DOI: [https://doi.org/10.1016/S0167-2991\(06\)81511-9](https://doi.org/10.1016/S0167-2991(06)81511-9)